Robust Radiometric Calibration for Dynamic Scenes in the Wild (Supplemental material)

Implementation Details for solving the optimization problem:

Here, we explain the details of our optimization method, which uses outlier rejection procedure proposed by Lee et al. [1]. We modify the Eq 6. from our paper to explain the optimization procedure:

$$\hat{g} = \arg\min_{g} \sum_{i=1}^{N-m+1} \left(\text{rank}(Y_i) + \text{rank}(Y_i')\right) + \lambda \sum_{t} H\left(-\frac{\partial g(t)}{\partial B}\right) \tag{1}$$

$$\text{s.t.}\;\; Y_i = g \circ D_i,\;\; Y_i' = g \circ D_i'$$

The following inverse camera response function (CRF) estimation procedure takes input as observation matrices D_i and D_i' and returns inverse CRF. The construction of observation matrices is explained in the paper.

Algorithm Inverse Camera Response Function Estimation

1: **procedure** RobustRadCalib($D_1, D_1', \cdots, D_i, D_i', \cdots, D_{N-m+1}, D'_{N-m+1}$)
2:     Initialize g
3:     **while** not converged **do**
4:         **for** $\boldsymbol{i} \leftarrow 1$ $\boldsymbol{to}$ $N-m+1$
5:             $X_i = g \circ D_i$
6:             $X_i' = g \circ D_i'$
7:             $Y_i = OutlierRejection(X_i, rho)$
8:             $Y_i' = OutlierRejection(X_i', rho)$
9:         **end for**
10:         Calculate error using Eq. 1
11:         Update g
12:     **end while**
13:     **return** $\hat{g}$
14: **end procedure**

The above procedure calculates the inverse camera response function g given set of observation matrices. For line 7 and 8 we use the outlier rejection procedure given in Lee et al. [1]. In line 2, we initialize g to a linear function. Note that in Eq.1 we use second condition number instead of rank as explained in Sec. 3.1.1. We use Levenberg-Marquardt method to update g in line 11.

Data distribution for synthetic dataset

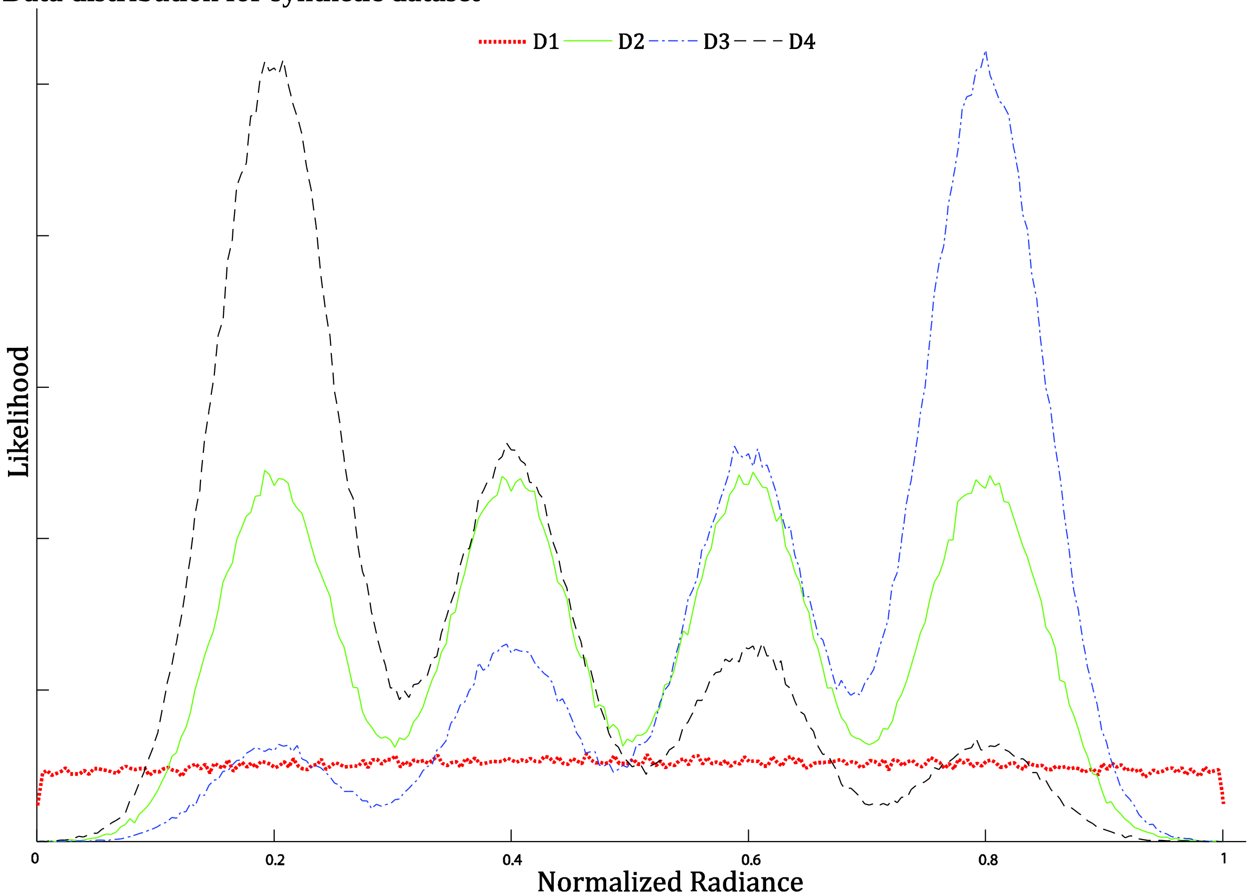

Simulations on real dataset:

We now present RMSE performance for different radiometric calibration methods for each real exposure set from our dataset. We compare against the methods of Grossberg and Nayar [2] (GN), Mitsunga and Nayar [3] (MN), Lee et al. [1]. First we show the results for the entire real dataset:

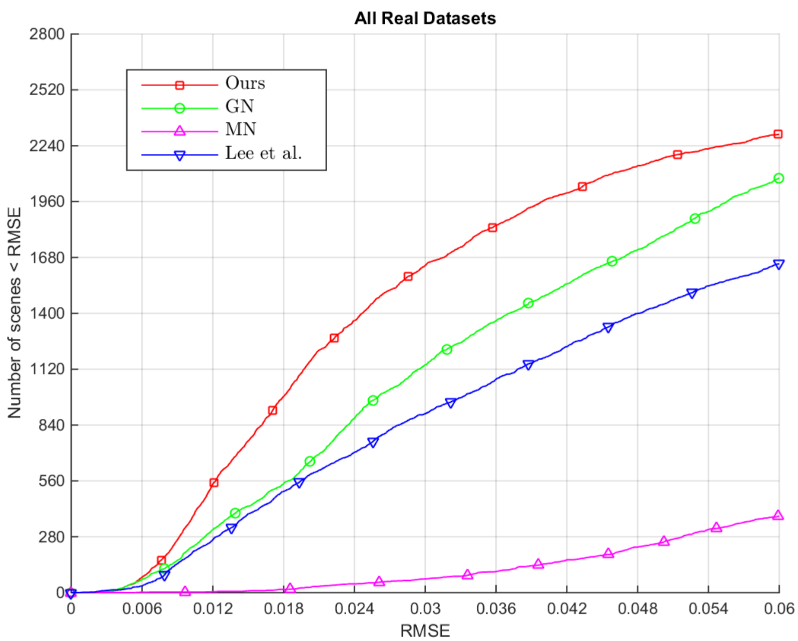

We show cumulative histogram of number of successful cases for different radiometric calibration methods w.r.t. RMSE for the entire real dataset. Our method shows significant improvement over the previous approaches of Grossberg and Nayar (GN), Mitsunga and Nayar (MN) and Lee et al.

1)

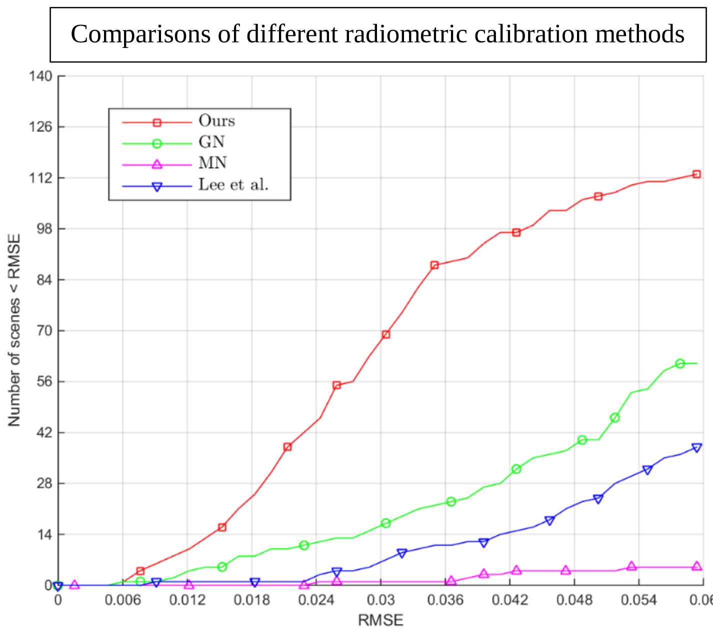

Comparisons of different radiometric calibration methods
Ours
GN
MN
Lee et al.
Number of scenes < RMSE
RMSE
140
126
112
98
84
70
56
42
28
14
0
0
0.006
0.012
0.018
0.024
0.03
0.036
0.042
0.048
0.054
0.06

2)

Comparisons of different radiometric calibration methods

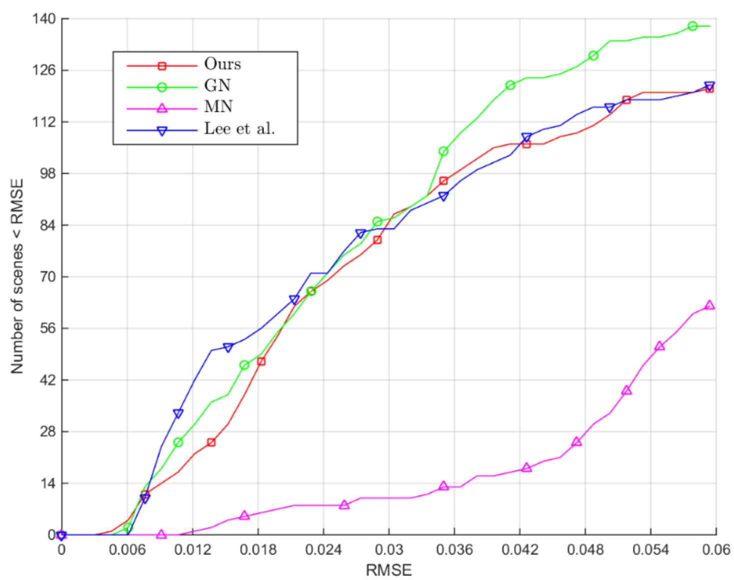

3)

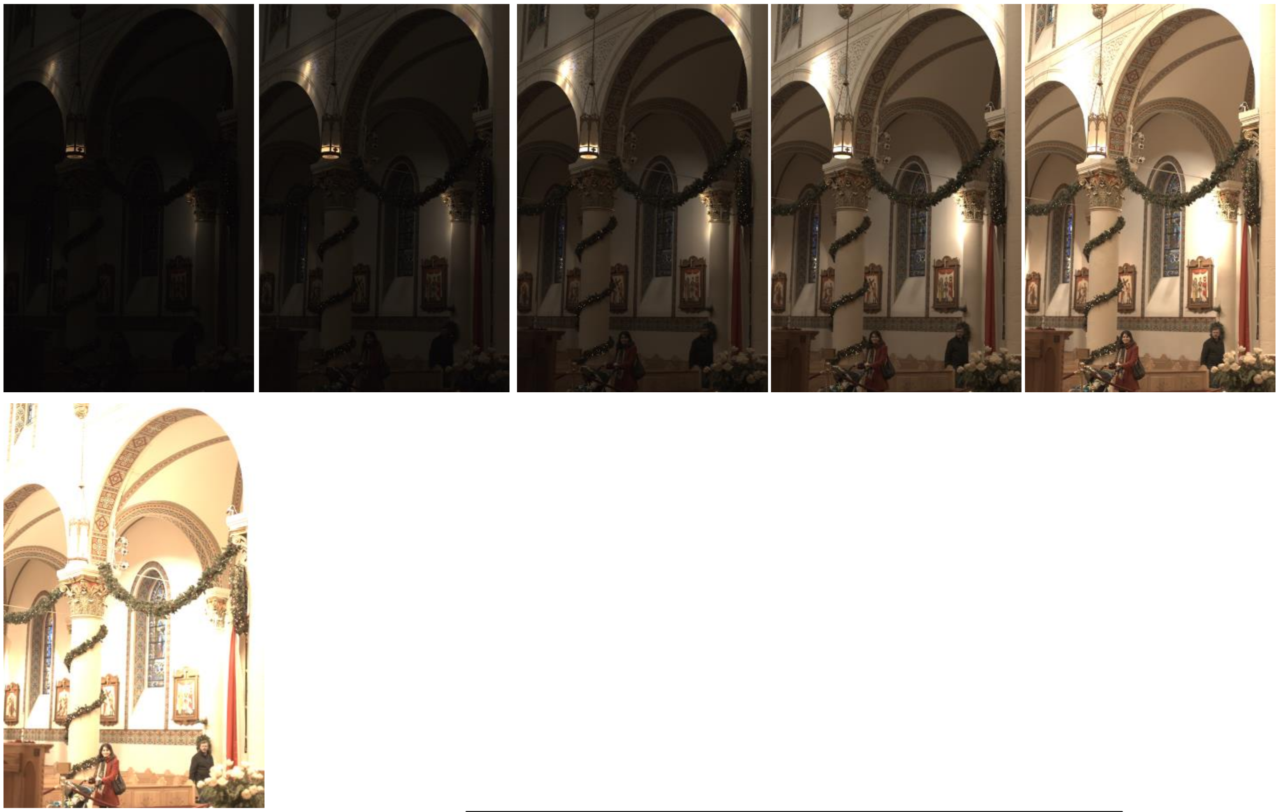

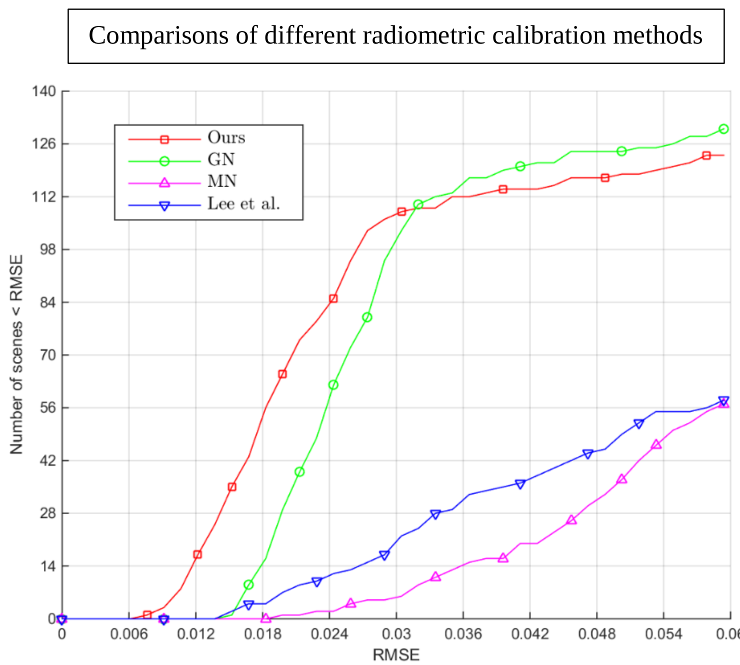
Comparisons of different radiometric calibration methods
Ours
GN
MN
Lee et al.
Number of scenes < RMSE
RMSE
0
14
28
42
56
70
84
98
112
126
140
0
0.006
0.012
0.018
0.024
0.03
0.036
0.042
0.048
0.054
0.06

4)

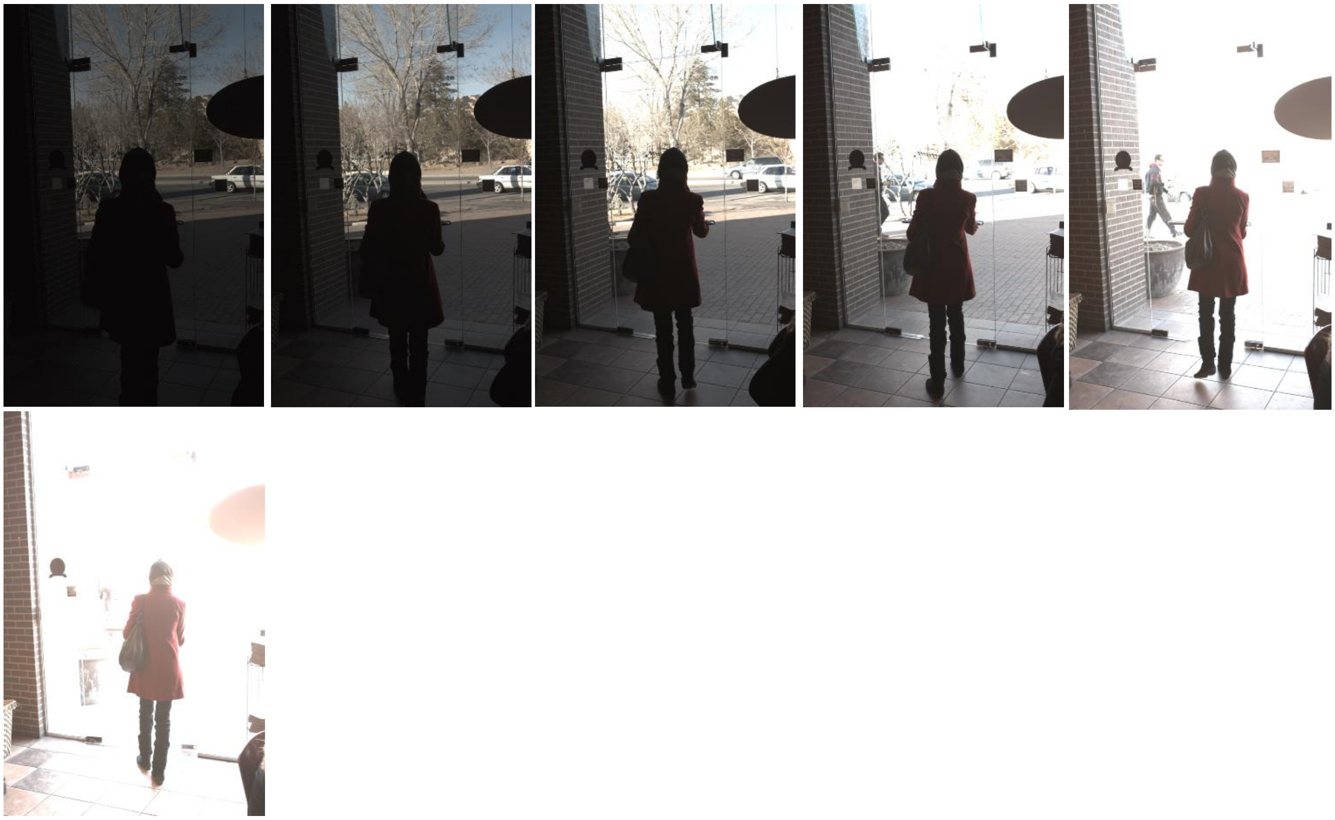

Comparisons of different radiometric calibration methods

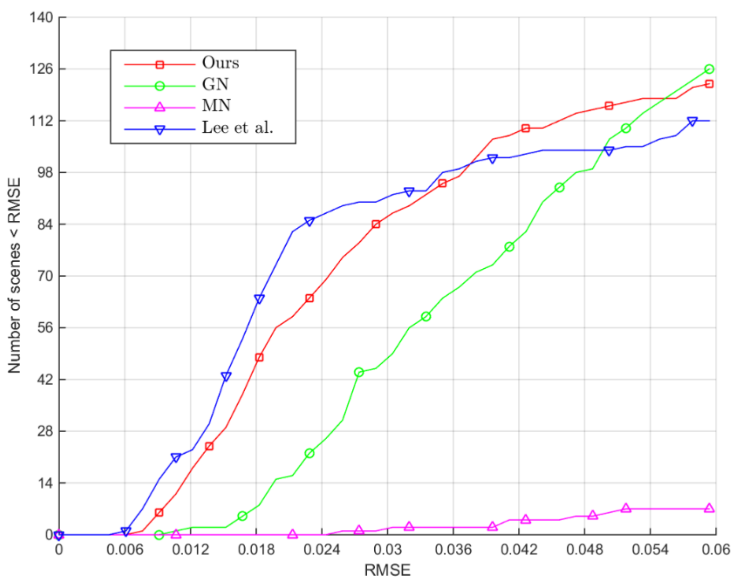

5)

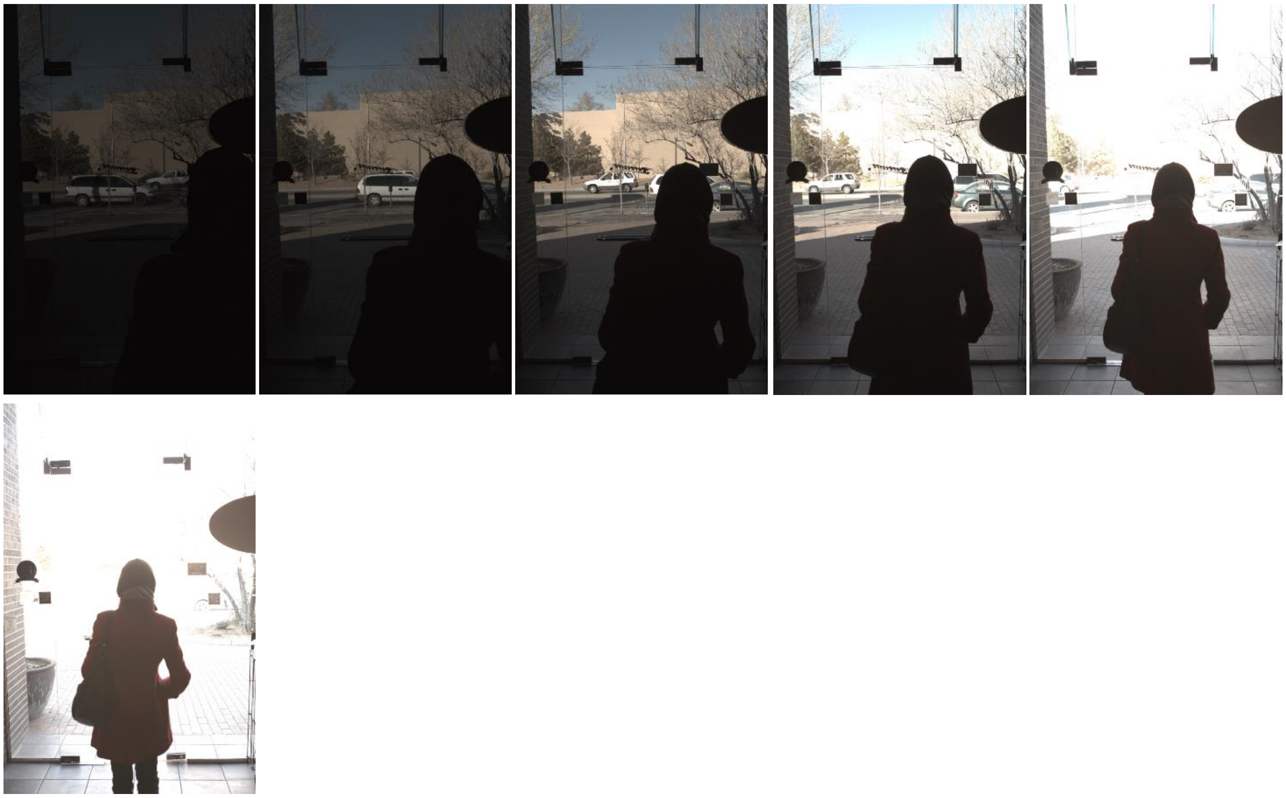

Comparisons of different radiometric calibration methods

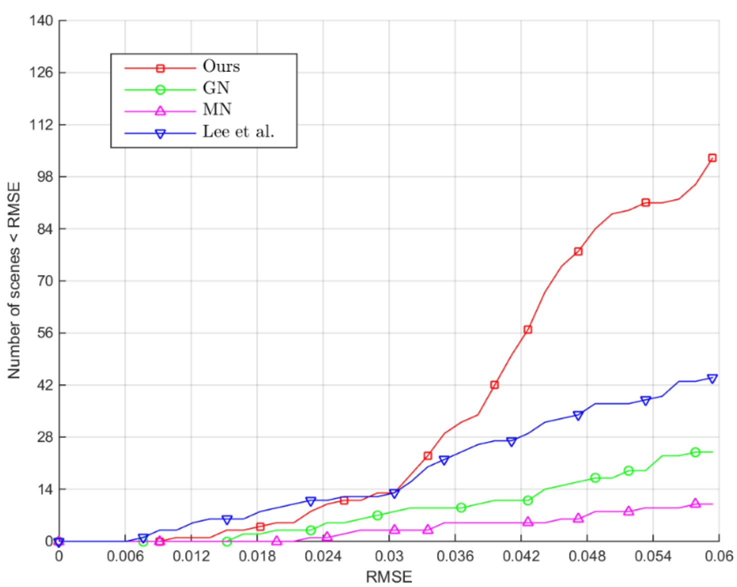

6)

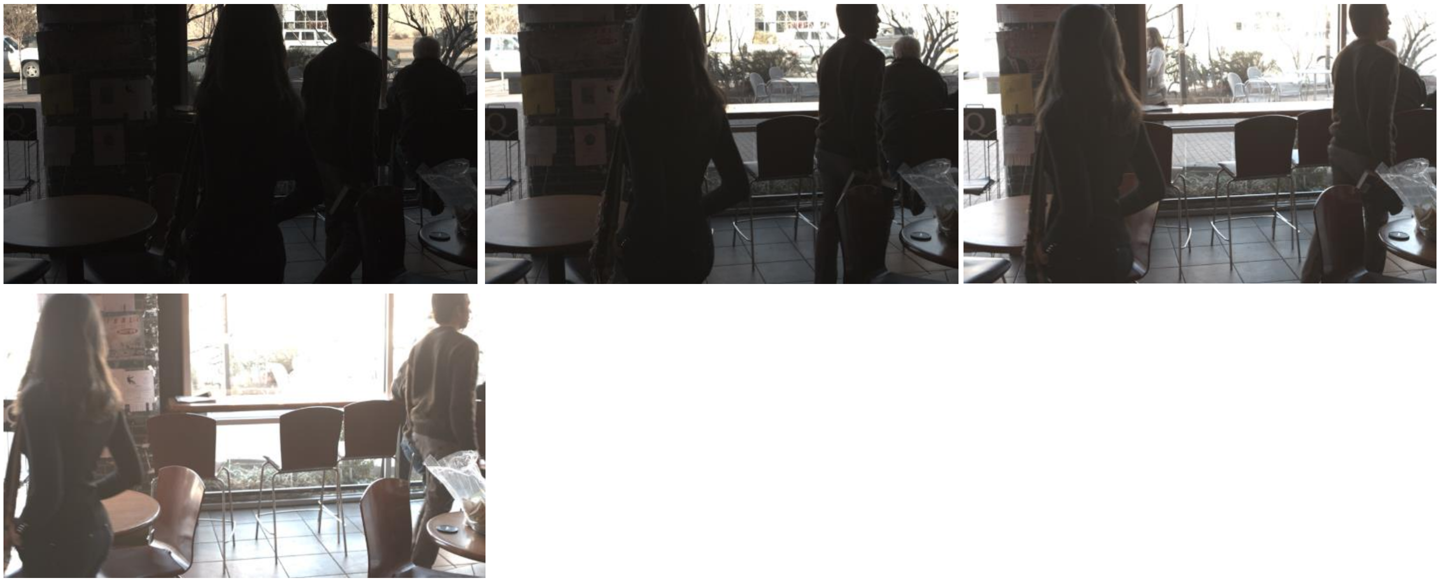

Comparisons of different radiometric calibration methods

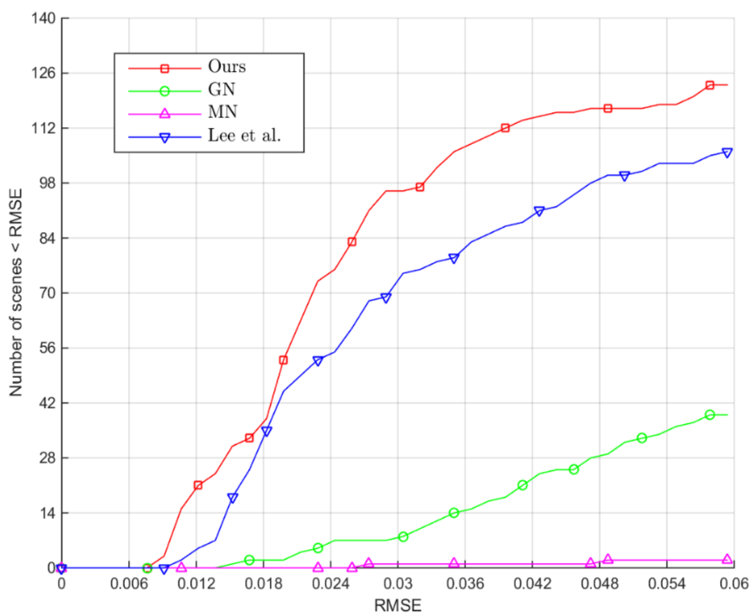

7)

Comparisons of different radiometric calibration methods

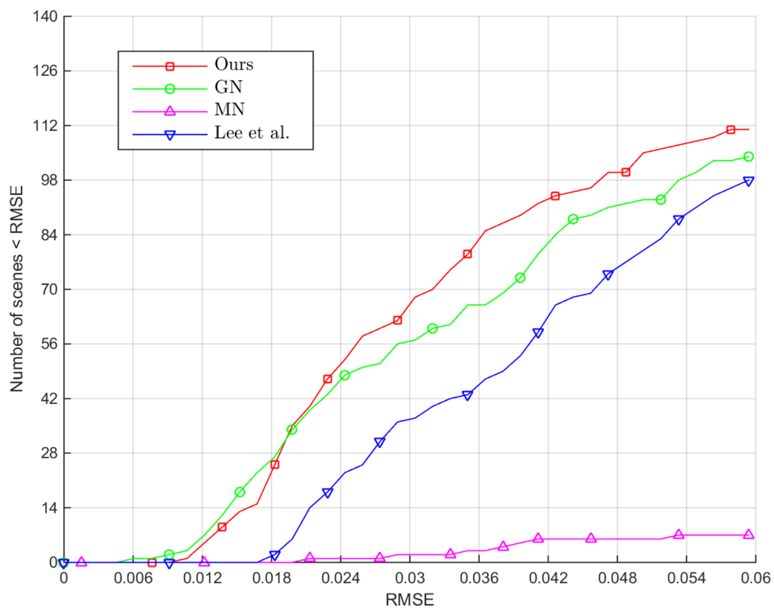

8)

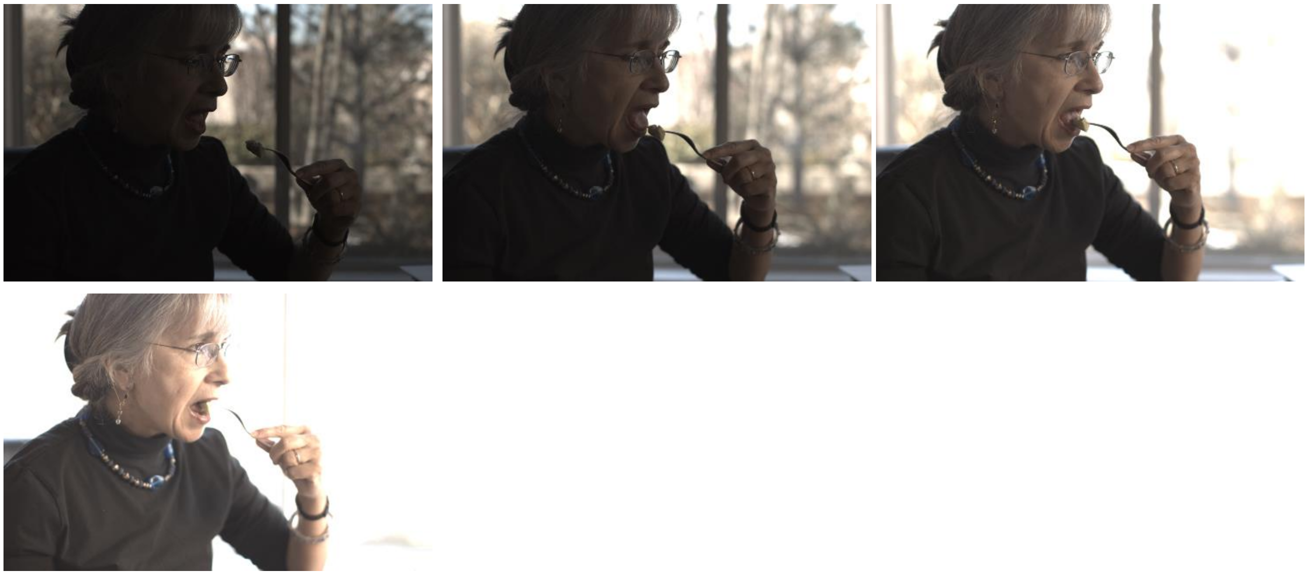

Comparisons of different radiometric calibration methods

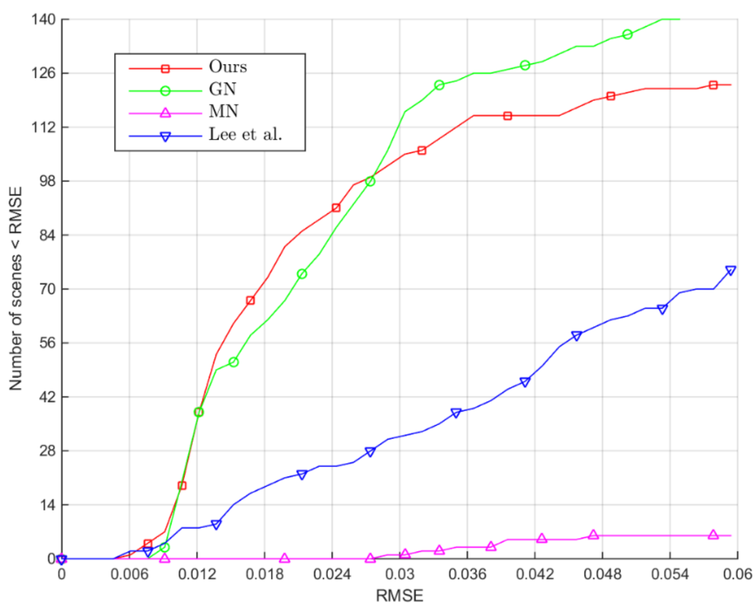

9)

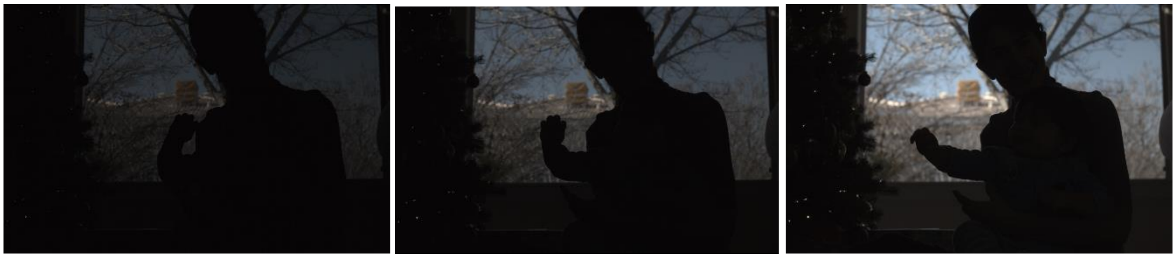

Comparisons of different radiometric calibration methods

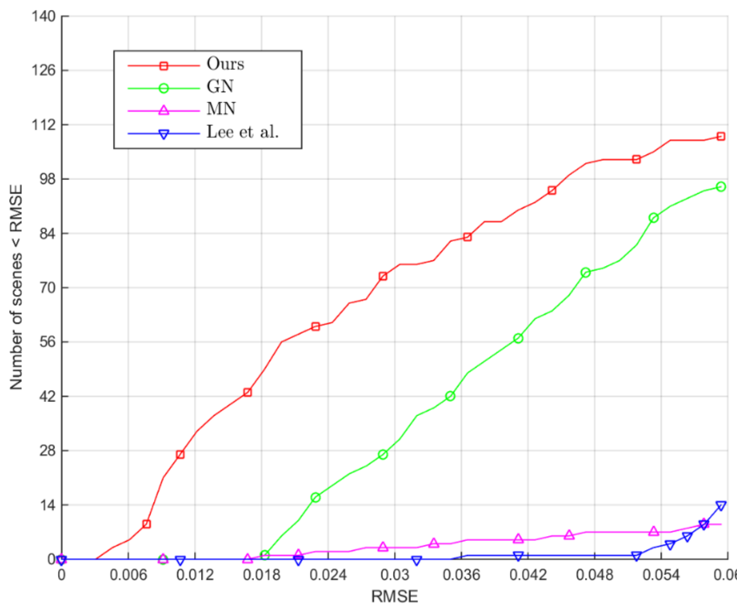

10)

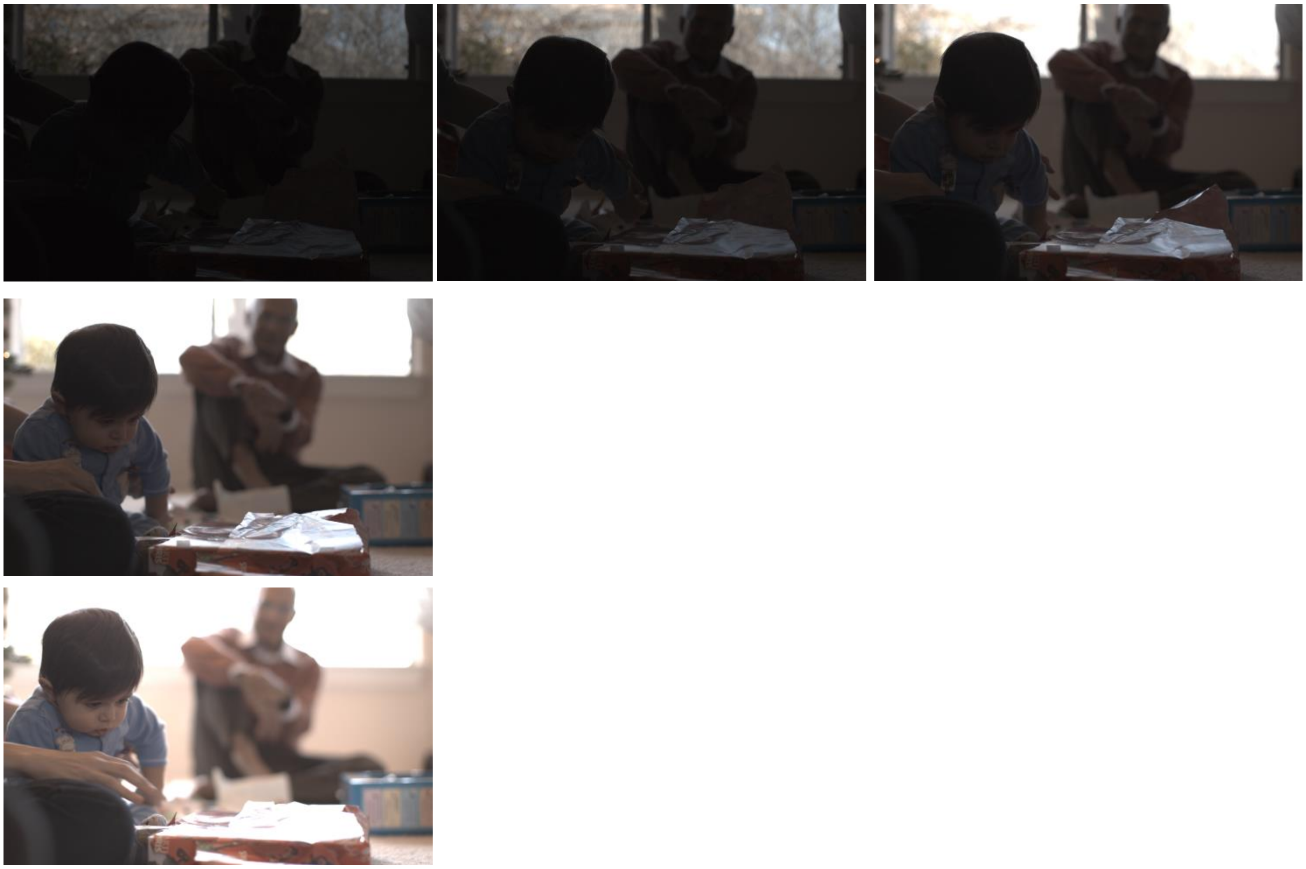

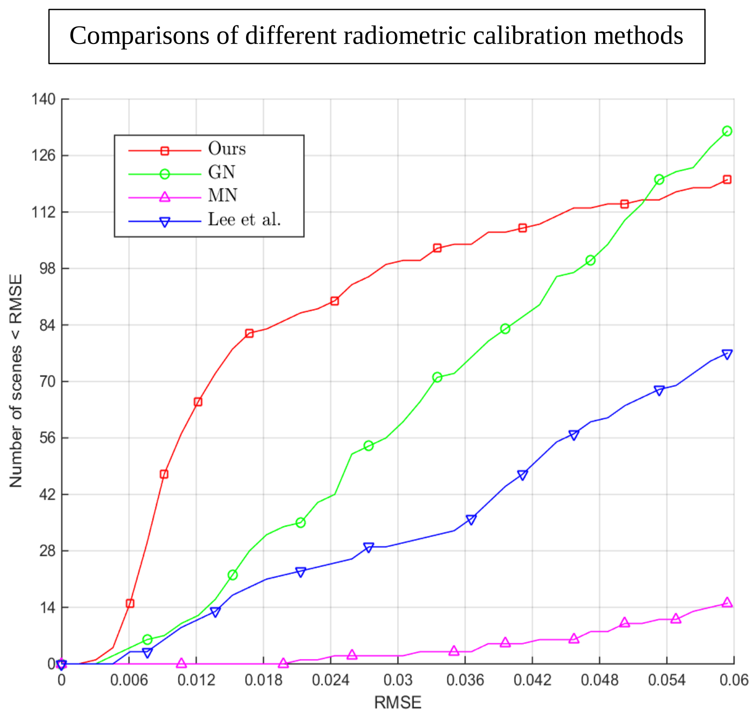
Comparisons of different radiometric calibration methods
Ours
GN
MN
Lee et al.
Number of scenes < RMSE
RMSE
0
14
28
42
56
70
84
98
112
126
140
0
0.006
0.012
0.018
0.024
0.03
0.036
0.042
0.048
0.054
0.06

11)

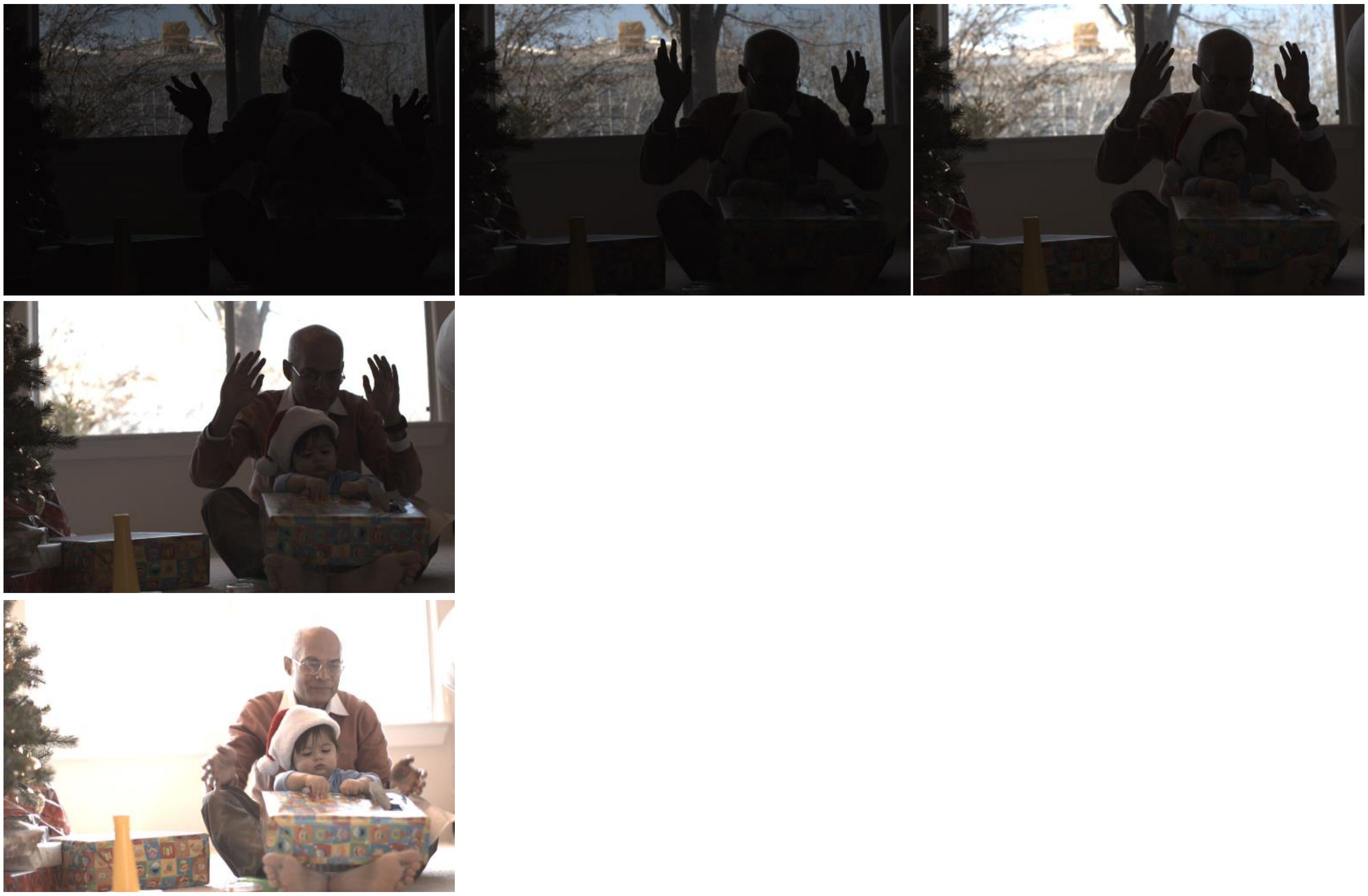

Comparisons of different radiometric calibration methods

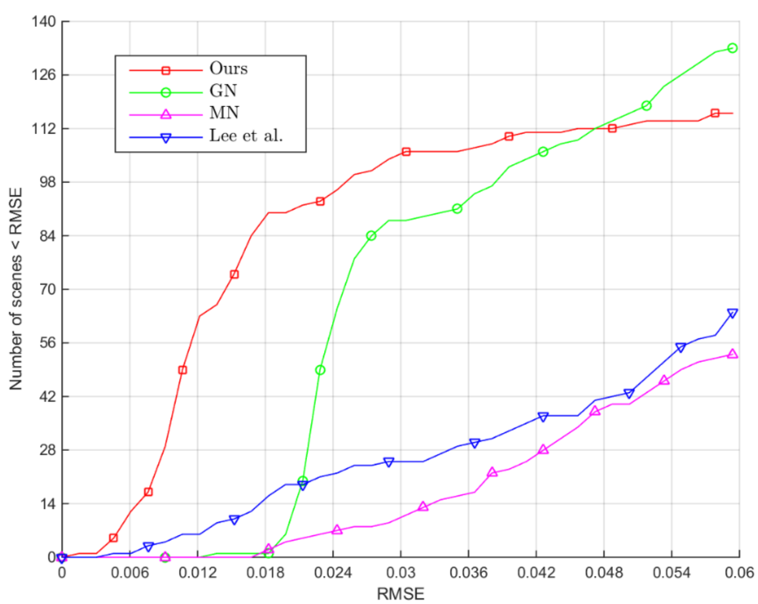

12)






Comparisons of different radiometric calibration methods

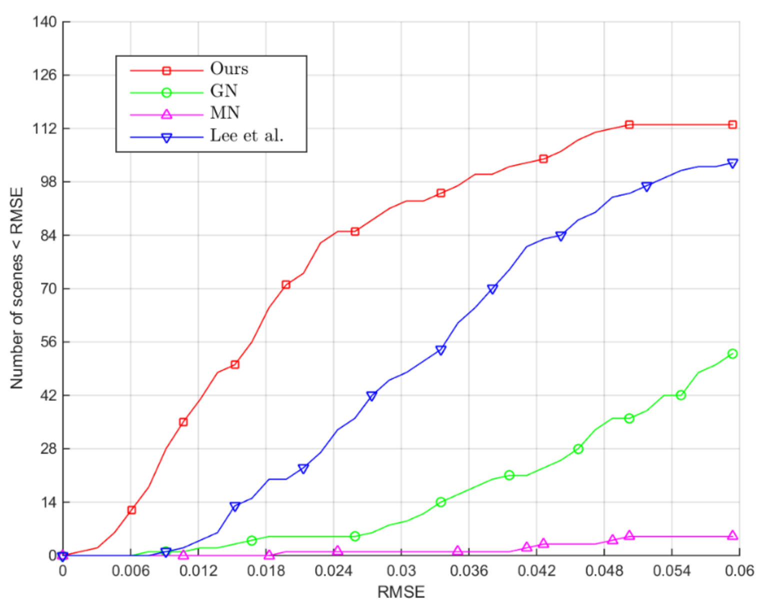

13)

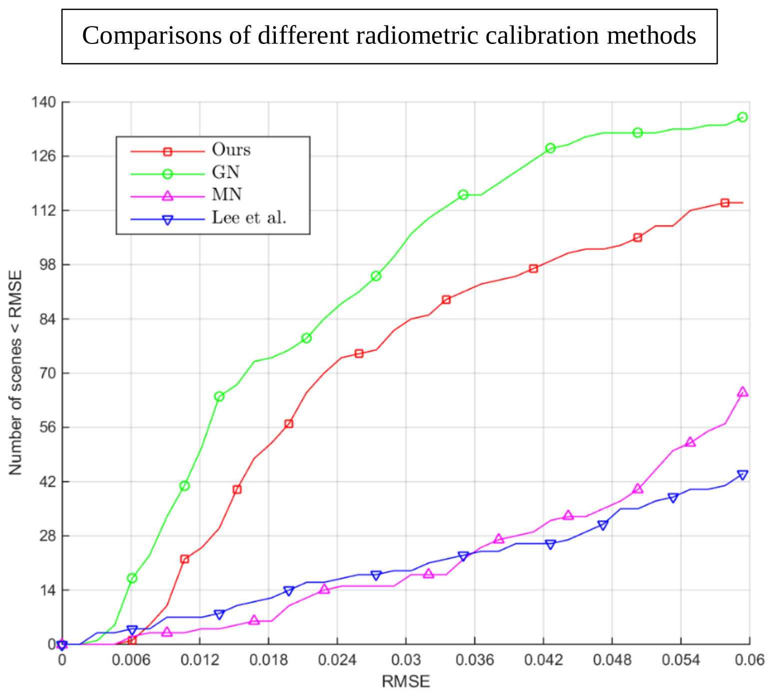

Comparisons of different radiometric calibration methods
Ours
GN
MN
Lee et al.
Number of scenes < RMSE
RMSE
140
126
112
98
84
70
56
42
28
14
0
0.006
0.012
0.018
0.024
0.03
0.036
0.042
0.048
0.054
0.06

14)

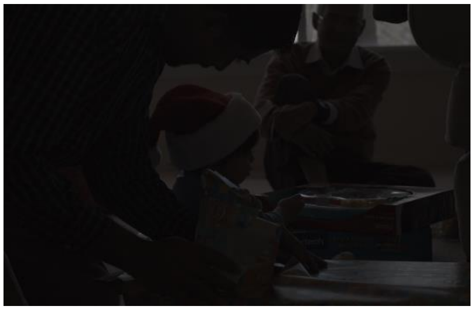



Comparisons of different radiometric calibration methods

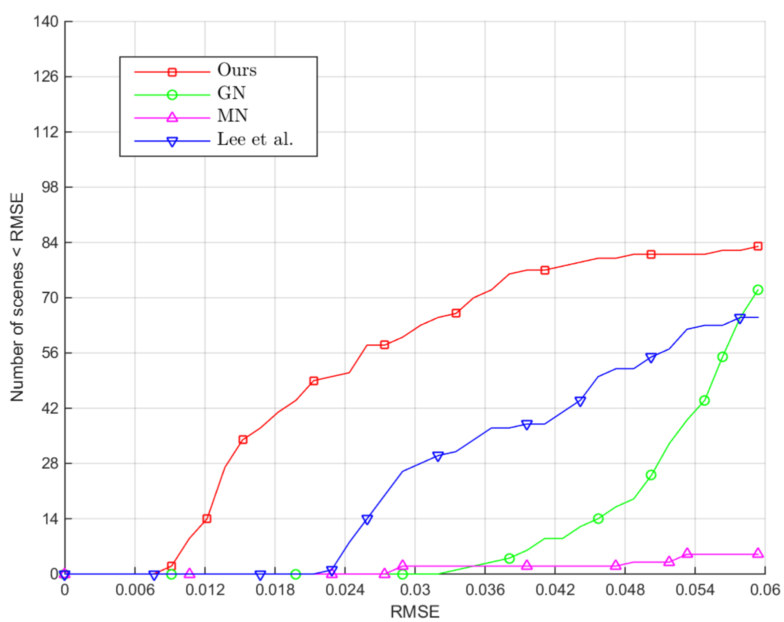

15)

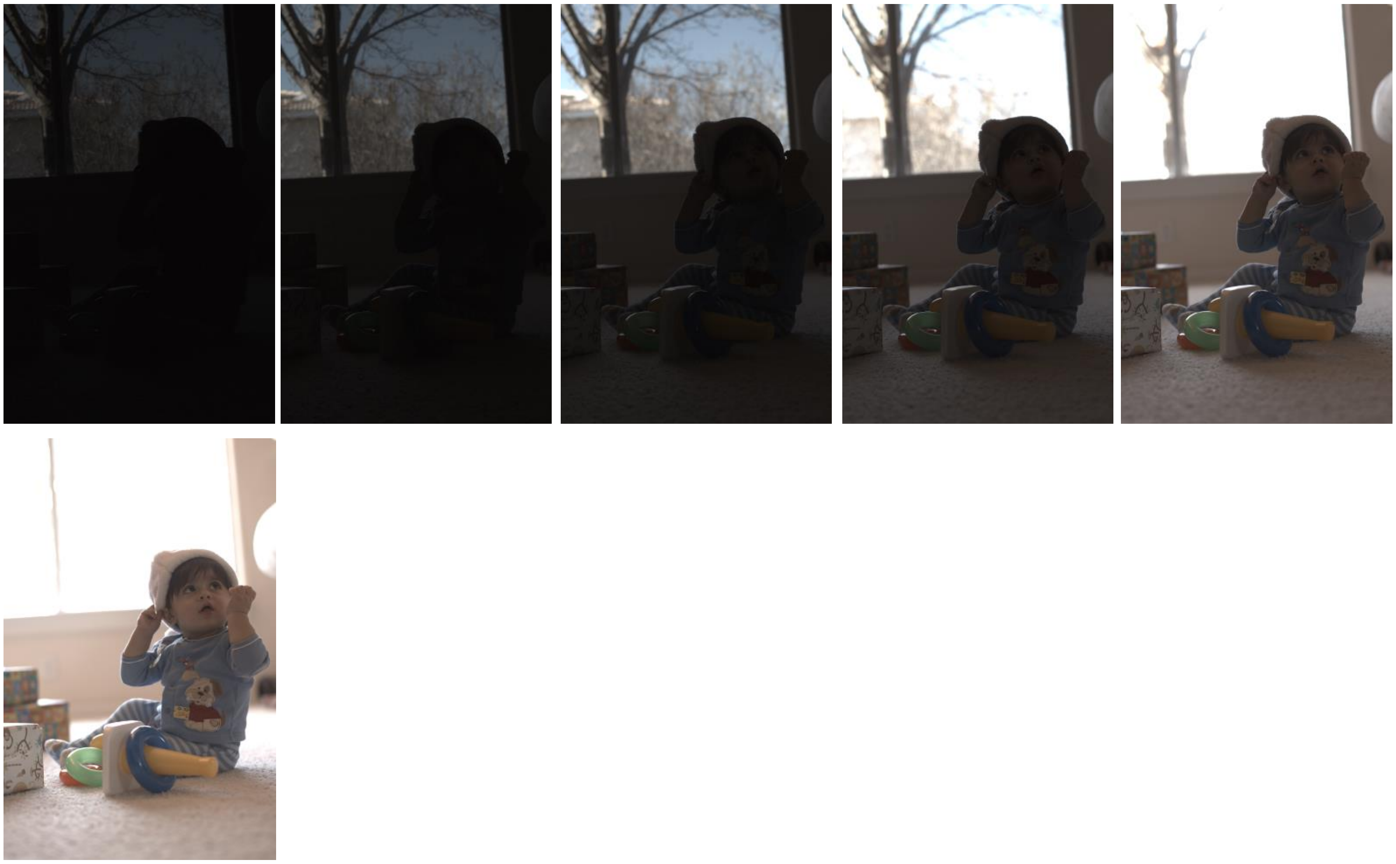

Comparisons of different radiometric calibration methods

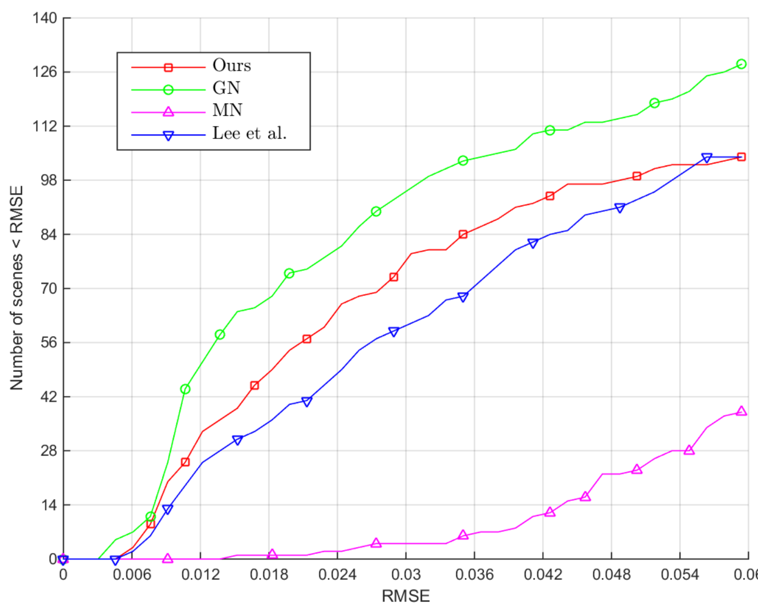

16)

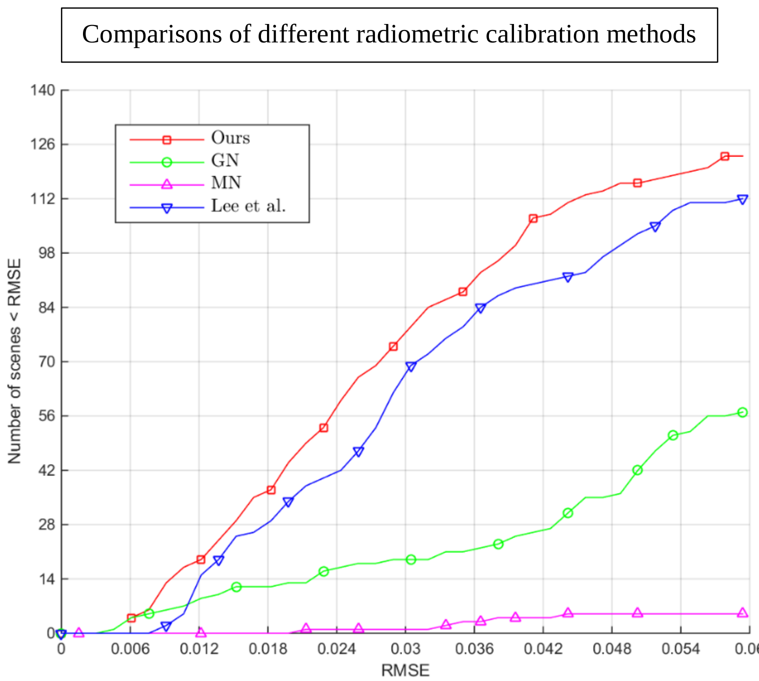
Comparisons of different radiometric calibration methods
Ours
GN
MN
Lee et al.
Number of scenes < RMSE
RMSE
0
14
28
42
56
70
84
98
112
126
140
0.006
0.012
0.018
0.024
0.03
0.036
0.042
0.048
0.054
0.06

17)

Comparisons of different radiometric calibration methods

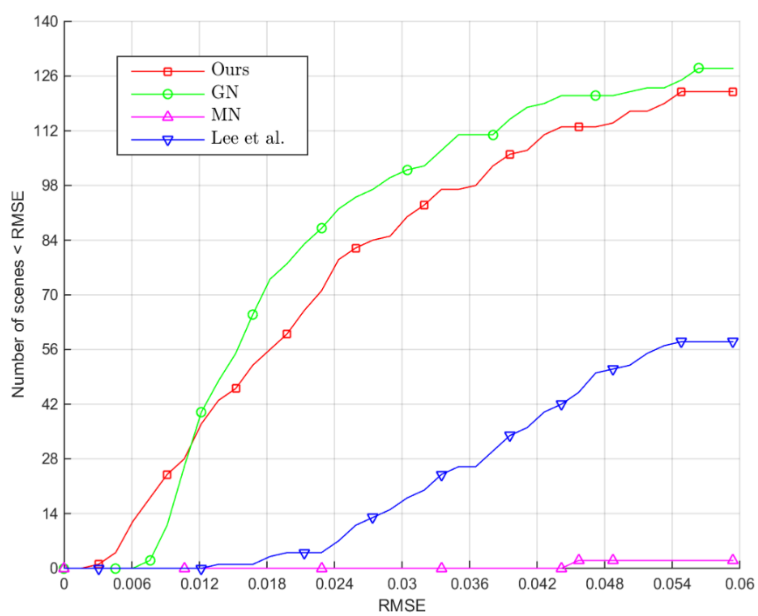

18)

Comparisons of different radiometric calibration methods

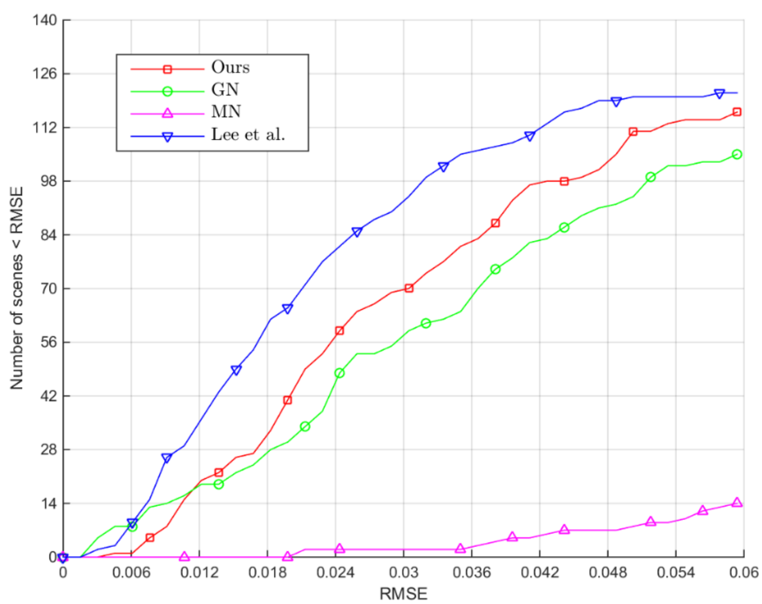

19)

Comparisons of different radiometric calibration methods

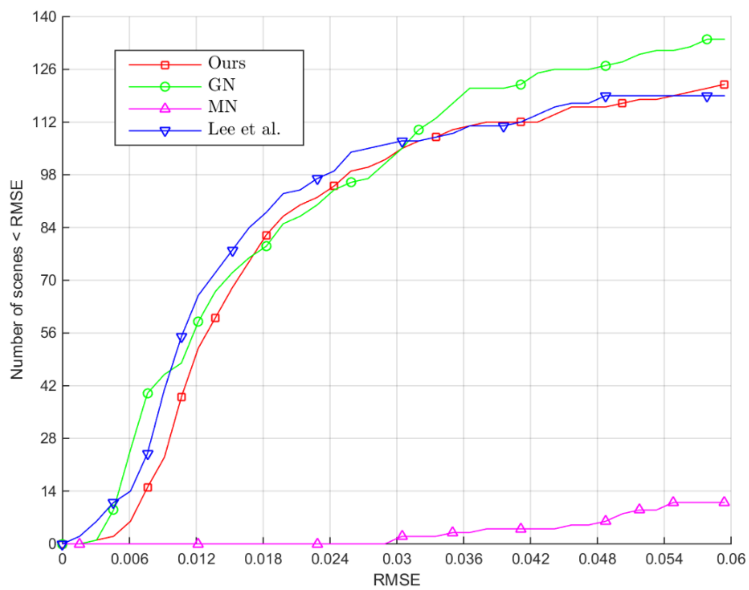

20)

Comparisons of different radiometric calibration methods

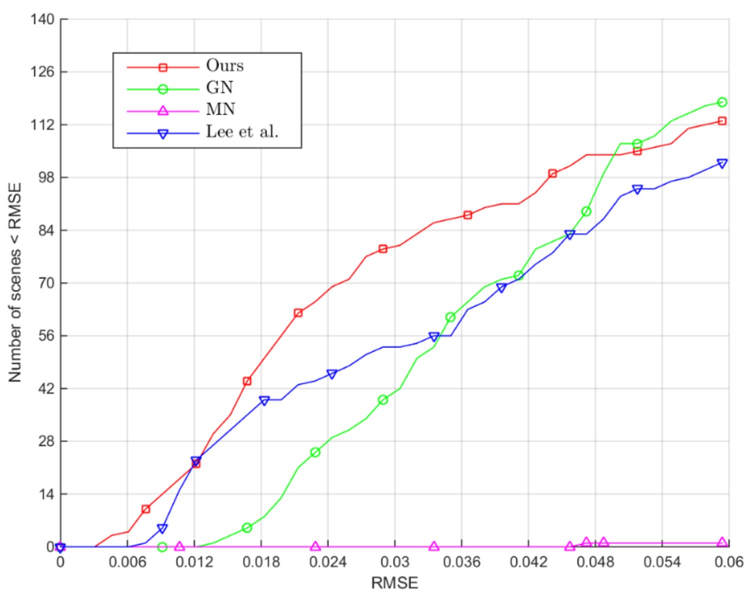

Discussions:

We have designed our proposed approach to achieve robust radiometric calibration performance for dynamic scenes in the wild. As can be seen from above results that our proposed approach performed consistently well on all the real exposure sets. In some of the test cases, Grossberg and Nayar's method performed slightly better than ours. This could happen when the intensity mapping functions (IMF) have less inaccuracies. In case of accurate IMF estimation, least squares approach of Grossberg and Nayar's recovers the inverse camera response function with good accuracy. However, on the other hand, when the IMF estimation is not accurate, least square approach overfits to the inaccuracies and we get very poor results as shown in some of the examples above.

Overall, our proposed radiometric calibration approach was very robust on the real dataset and performed consistently well. On the other hand, other radiometric calibration approaches, performed well in some test cases but very poorly on others.

Application to High Dynamic Range (HDR) Imaging:

We used our radiometric calibration method as a preprocessing step to HDR image reconstruction method by Sen et al. [4]. Their algorithm assumes that input LDR images are linear in nature and that the exposure ratios between the LDR images is known and given. Given a set of input LDR images (in 'jpeg' or any non-linear format and exposure ratios are not known), we first estimate the inverse camera response function up to an exponential ambiguity. We solve this ambiguity by adding constraints as shown in Eq. 8 in Sec 5. We also recover the pseudo exposure ratios. Hence, given a set of LDR images, we first recover linear LDR images by applying inverse camera response function. We use these linear LDR images and estimated pseudo exposure ratios as inputs to Sen et al.'s [4] HDR image reconstruction method.

Following are couple of examples of HDR image reconstructed using above approach:

Input LDRs are obtained from Kang et al. [5]

LDR images

HDR image

Input LDRs are obtained from Hu et al. [7]

LDR images

HDR image

Input LDRs are obtained from Granados et al. [6]

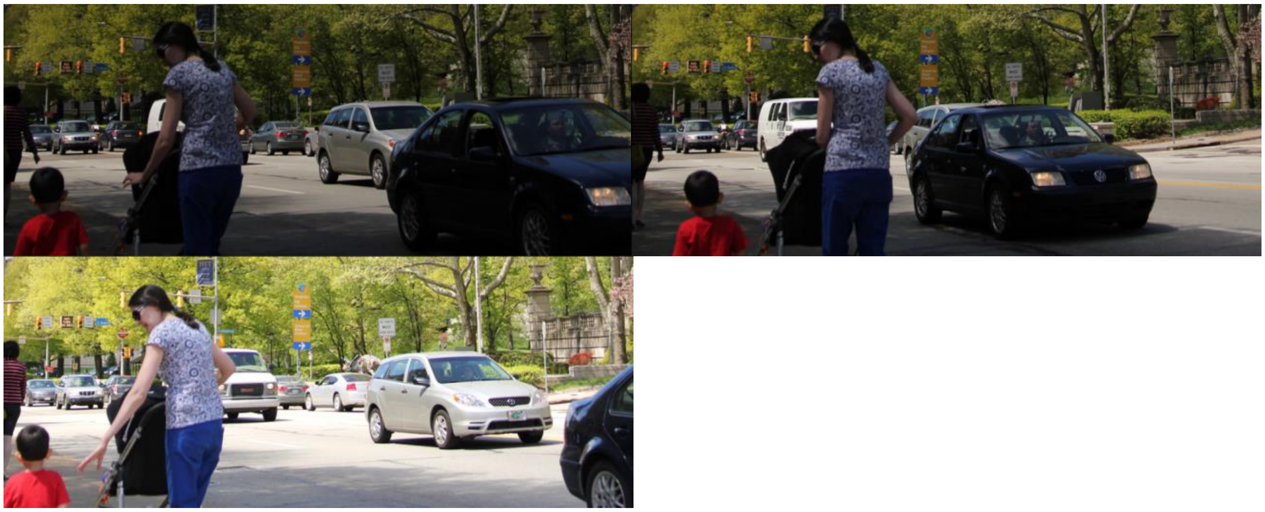

LDR images

HDR image

REFERENCES:

[1] Joon-Young Lee; Matsushita, Y.; Boxin Shi; In So Kweon; Ikeuchi, K., "Radiometric Calibration by Rank Minimization," *Pattern Analysis and Machine Intelligence, IEEE Transactions on* , vol.35, no.1, pp.144,156, Jan. 2013

[2] Grossberg, M.D.; Nayar, S.K., "Determining the camera response from images: what is knowable?," *Pattern Analysis and Machine Intelligence, IEEE Transactions on* , vol.25, no.11, pp.1455,1467, Nov. 2003

[3] Mitsunaga, T.; Nayar, S.K., "Radiometric self calibration," *Computer Vision and Pattern Recognition, 1999. IEEE Computer Society Conference on.* , vol.1, no., pp.,380 Vol. 1, 1999

[4] Pradeep Sen, Nima Khademi Kalantari, Maziar Yaesoubi, Soheil Darabi, Dan B. Goldman, and Eli Shechtman. 2012. Robust patch-based hdr reconstruction of dynamic scenes. *ACM Trans. Graph.*31, 6, Article 203 (November 2012)

[5] Sing Bing Kang, Matthew Uyttendaele, Simon Winder, and Richard Szeliski. 2003. High dynamic range video. *ACM Trans. Graph.* 22, 3 (July 2003), 319-325.

[6] Miguel Granados, Kwang In Kim, James Tompkin, and Christian Theobalt. 2013. Automatic noise modeling for ghost-free HDR reconstruction. *ACM Trans. Graph.* 32, 6, Article 201 (November 2013)

[7] Jun Hu; Gallo, O.; Pulli, K.; Xiaobai Sun, "HDR Deghosting: How to Deal with Saturation?," *Computer Vision and Pattern Recognition (CVPR), 2013 IEEE Conference on* , vol., no., pp.1163,1170, 23-28 June 2013